TISSUE ENGINEERING: Part A
Volume 21, Numbers 9 and 10, 2015

DOI: 10.1089/ten.tea.2014.0426

Autologously Generated Tissue-Engineered Bone Flaps for Reconstruction of Large Mandibular Defects in an Ovine Model

Alexander M. Tatara, BS,[1] James D. Kretlow, MD, PhD,[1] Patrick P. Spicer, MD, PhD,[1] Steven Lu, BS,[1] Johnny Lam, BS,[1] Wei Liu, MD, PhD,[2] Yilin Cao, MD, PhD,[2] Guangpeng Liu, PhD,[2] John D. Jackson, PhD,[3] James J. Yoo, MD, PhD,[3] Anthony Atala, MD,[3] Jeroen J.J.P. van den Beucken, PhD,[4] John A. Jansen, DDS, PhD,[4] F. Kurtis Kasper, PhD,[1] Tang Ho, MD,[5] Nagi Demian, MD,[6] Michael John Miller, MD,[7] Mark E. Wong, DDS,[6] and Antonios G. Mikos, PhD[1]

The reconstruction of large craniofacial defects remains a significant clinical challenge. The complex geometry of facial bone and the lack of suitable donor tissue often hinders successful repair. One strategy to address both of these difficulties is the development of an *in vivo* bioreactor, where a tissue flap of suitable geometry can be orthotopically grown within the same patient requiring reconstruction. Our group has previously designed such an approach using tissue chambers filled with morcellized bone autograft as a scaffold to autologously generate tissue with a predefined geometry. However, this approach still required donor tissue for filling the tissue chamber. With the recent advances in biodegradable synthetic bone graft materials, it may be possible to minimize this donor tissue by replacing it with synthetic ceramic particles. In addition, these flaps have not previously been transferred to a mandibular defect. In this study, we demonstrate the feasibility of transferring an autologously generated tissue-engineered vascularized bone flap to a mandibular defect in an ovine model, using either morcellized autograft or synthetic bone graft as scaffold material.

Introduction

Large mandibular defects pose substantial challenges to reconstructive surgeons due to several factors, including the aesthetic need to preserve the natural contours of the face, high infection rates due to proximity to the oral flora, and the significant size of the defects.[1,2] Furthermore, these patients often have additional complicating factors, such as irradiation of the site in oncologic patients and massive composite defects of soft tissue, nerve, and bone in trauma and military populations.[1,3,4] Most commonly, these defects are reconstructed with autograft (AG) bone as either a flap (transferred with native vasculature) or as a graft (without vasculature).[5] While flaps are preferred, flap harvest and transfer is more technically demanding than grafting and there are less available donor sites for potential flaps.[5–7] In either case, the donated tissue often does not conform to the geometry of the defect site and the surgeon will attempt to shape it as best as possible to retain facial aesthetics.

Due to the importance of the shape of the donor tissue and the lack of potential donor sites, autologously generated flaps from *in vivo* bioreactors have been explored as an alternative tissue source for large craniofacial defects.[8] *In vivo* bioreactors are chambers and/or scaffolds placed in an orthotopic site in the patient's body where tissue can be grown and harvested for later transfer.[9] This *in vivo* bioreactor approach particularly lends itself to the two-stage mandibular reconstruction strategy, as new tissue can be grown in the bioreactor while a space maintenance device preserves the anatomical planes within the mandibular defect.[10] In combination with growth factors and scaffold material, the *in vivo* bioreactor approach has been utilized in humans to repair large mandibular defects in pilot studies.[11–13] However, the introduction of growth factors to a system for use in the craniofacial region carries risks of tissue overgrowth, nerve impingement, and additional regulatory challenges.[14] To that effect, strategies utilizing *in vivo* bioreactors without exogenous growth factors are

[1]Department of Bioengineering, Rice University, Houston, Texas.
[2]Department of Plastic and Reconstructive Surgery, Shanghai 9th People's Hospital, Shanghai Jiao Tong University School of Medicine, Shanghai, China.
[3]Wake Forest Institute for Regenerative Medicine, Wake Forest University Health Sciences, Winston-Salem, North Carolina.
[4]Department of Biomaterials, Radboud UMC, Nijmegen, The Netherlands.
[5]Department of Otorhinolaryngology, University of Texas Medical School at Houston, Houston, Texas.
[6]Department of Oral and Maxillofacial Surgery, University of Texas Dental Branch at Houston, Houston, Texas.
[7]Department of Plastic Surgery, Ohio State University, Columbus, Ohio.

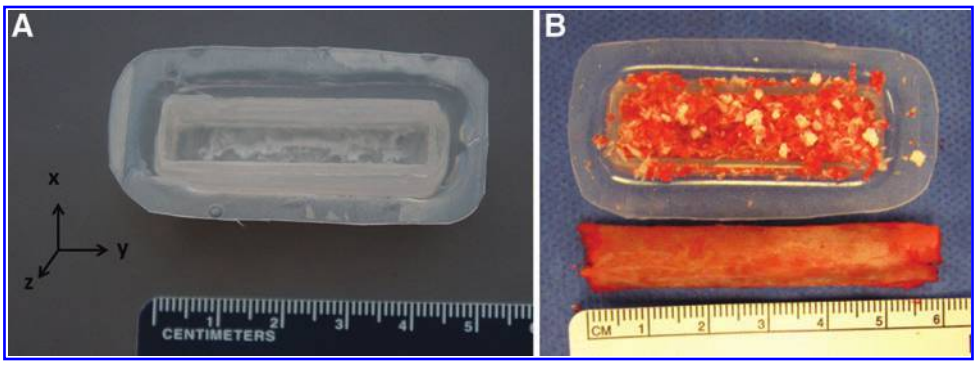

FIG. 1. **(A)** Poly(methyl methacrylate)-based tissue chamber. The open face (in the Z direction) is implanted against the periosteum. **(B)** A loaded tissue chamber with both synthetic bone graft and morcellized autograft. Below is an excised portion of the rib that is removed to generate morcellized autograft and to generate space for chamber implantation.

being explored. Specifically, poly(methyl methacrylate) (PMMA)-based chambers have been filled with different scaffold materials and implanted against the periosteum of sheep rib for tissue generation.[15–19] After tissue ingrowth, the chamber can be harvested with the accompanying intercostal artery and vein, resulting in a flap that matches the dimension of the implanted tissue chamber.[15,19] While morcellized autologous bone graft, devitalized autograft, and poly(lactic-*co*-glycolic acid) scaffolds have all been explored previously as scaffold material, autograft resulted in the greatest amount of generated bone.[16,18] In addition, these tissue chambers have been harvested from the rib at different time points, and 9 weeks has been established as an optimal time for ossified tissue growth.[16,19] This approach has been successful in generating vascularized bone flaps in both a sheep model[15–19] and in a reported clinical case.[20] Although this system has been shown to be successful in generating ossified tissue with specific dimensions, this tissue had not previously been transferred to a defect in the sheep model.

While morcellized autograft bone may be beneficial due to endogenous growth factors within the extracellular matrix, its harvest increases donor site morbidity. It may be possible that the combination of synthetic bone graft with autograft can reduce the amount of donor tissue needed for the scaffold within the bioreactor. Synthetic ceramic bone grafts are currently available to clinicians to aid in the reconstruction of defects as cellular scaffold material.[21,22] For example, biphasic ceramic synthetic graft (SG) materials can be composed of different ratios of beta-tricalcium phosphate and hydroxyapatite and have shown efficacy in the repair of craniofacial bone.[23,24] Therefore, in this feasibility study, tissue chambers were filled with different ratios of synthetic graft particles (85% beta-tricalcium phosphate/15% hydroxyapatite) to morcellized rib autograft and implanted against the periosteum of sheep rib. These tissue chambers were harvested after 9 weeks of growth and evaluated by microcomputed tomography (μCT) and histology to determine the effect of initial synthetic graft incorporation on the quantity and quality of tissue growth. In three animals, the contents of these *in vivo* bioreactors were transferred as vascularized free flaps to a mandibular angle defect. After 12 additional weeks, these mandibles were harvested and histologically evaluated to determine the viability of the tissue and integration with the native bone. Overall, the objective of this work was to determine the feasibility of transferring tissue generated from an *in vivo* bioreactor to a mandibular defect as a vascularized free flap and to evaluate the effect of synthetic bone graft on tissue growth.

Materials and Methods

Sheep and tissue chambers

Four female Dorset sheep (age 4 months, weight 31–35 kg) were used in a protocol approved by the Wake Forest University Institutional Animal Care and Use Committee. Tissue chambers were prepared as described previously.[18] Briefly, these chambers were fabricated from PMMA in dimensions of $4 \times 1 \times 1$ cm (length × width × height), with a single open face (4×1 cm). An ethylene-vinyl acetate cuff (1 cm overhang) was heat-molded around a metal bar of the same dimensions ($4 \times 1 \times 1$ cm) so that the PMMA chamber fit tightly inside to allow for suturing around the chamber exterior (Fig. 1A).

The chambers were sterilized by ethylene oxide. Each sheep was assigned to receive four chambers filled with different proportions (V/V) of morcellized AG or SG (MasterGraft Resorbable Ceramic Granule®; Medtronic, Minneapolis, MN): (1) 100% AG, (2) 75% AG/25% SG, (3) 50% AG/50% SG, (4) 25% AG/75% SG, or (5) 100% SG. The four sheep were randomly assigned the chambers as shown in Table 1.

Chamber implantation

Sheep were anesthetized and intubated. Two incisions ($\sim$12 cm) were made on the left flank, parallel to rib orientation. Through these incisions, the rib periosteum was accessed. On alternating ribs, beginning with either the second or third rib, four rib sections (5–6 cm in length) were removed. These sections were placed in a bone mill (KLS Martin, Mühlheim, Germany) to generate morcellized autograft (Fig. 1B). The morcellized autograft was packed at a consistent volume (0.55 g/L) for each group.

Table 1. Tissue Chamber Initial Composition (%AG/%SG V/V)

Chamber number	*Sheep 1*	*Sheep 2*	*Sheep 3*	*Sheep 4*
Chamber 1	25/75	25/75	25/75	50/50
Chamber 2	75/25	100/0	100/0	50/50
Chamber 3	50/50	0/100	100/0	0/100
Chamber 4	0/100	75/25	75/25	100/0

AG, autograft; SG, synthetic graft.

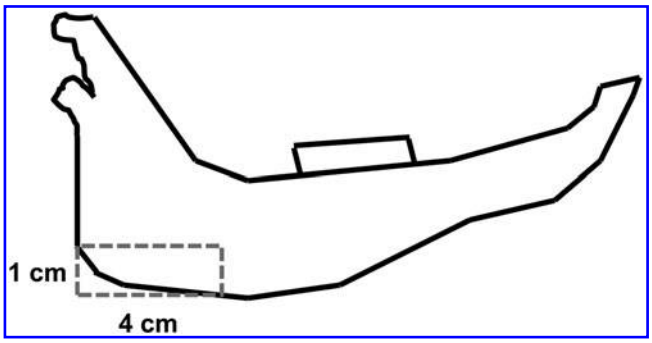

FIG. 2. Diagram of a sheep mandible. The *dashed box* represents the created angular defect.

These chambers were sewn to the periosteum of the rib with the open face in contact with the periosteal cambium. Chambers of 100% SG were wet with saline to minimize spillage during placement. In the case that the pleura was violated while removing a rib segment (occurred in one out of four animals), the pleura was repaired with a figure-of-eight stitch and the next alternating rib was used for the placement of the last chamber. After tissue chamber placement, the muscle, fascia, and skin were closed.

Chamber harvest and flap transfer

Nine weeks after implantation, the chambers were harvested with the animals under anesthesia. Briefly, the skin, fascia, and muscle were dissected for access to the ribs. Three of the chambers were removed by rongeur without pedicle. In three animals, the remaining chamber (100% SG, 100% AG, and 100% AG, respectively) was utilized as a flap for a created mandibular defect in the same animal from which the chamber was harvested. The intercostal artery and vein were isolated from one side of the flap, and the pedicle on the other side remained attached until the mandibular defect was prepared. This defect was created in the angle of the right mandible (4 cm in length × 1 cm in height) by using a dental bur (Fig. 2). An incision in the neck allowed for access to the great vessels and the flap was transferred into the defect. Anastomoses were performed under surgical microscopy (Leica Microsystems, Wetzlar, Germany) to attach the arterial (approximate diameter of 1.5 mm) and venous (approximate diameter of 0.5 mm) pedicles to a branch of the external carotid artery (transverse facial artery, internal maxillary artery, superficial temporal artery, or lingual artery depending on vessel size and availability) and accompanying vein in a side to side and end to side orientation. After confirming patency by observing pulsations, the flap was fixed by a small midface plate (KLS Martin) with standard bone screws and plating technique. The mandible and neck incisions were closed. The fourth sheep was euthanized for chamber harvest with no flap transfer. Harvested chamber contents were placed in 10% neutral buffered formalin for fixation.

Mandibular harvest

Twelve weeks following the transfer of the flap to the mandibular defect, the remaining three animals were euthanized for harvest of the mandibular angles. The mandibular angles and contralateral controls were removed by dental bur and fixed in 10% neutral buffered formalin for processing and analysis.

Microcomputed tomography

To perform nondestructive imaging and assessment of bone quality, a SkyScan 1172 microCT imaging system (SkyScan, Aartselaar, Belgium) was used to scan the tissue chamber specimens. Briefly, wet specimens were wrapped in parafilm and imaged with an X-ray tube voltage of 100 kV and current of 100 μA. Volumetric reconstruction and analysis was conducted using the software NRecon and CTAn as provided by SkyScan with 50% beam-hardening correction and a binary threshold of 40–255 with voxel size

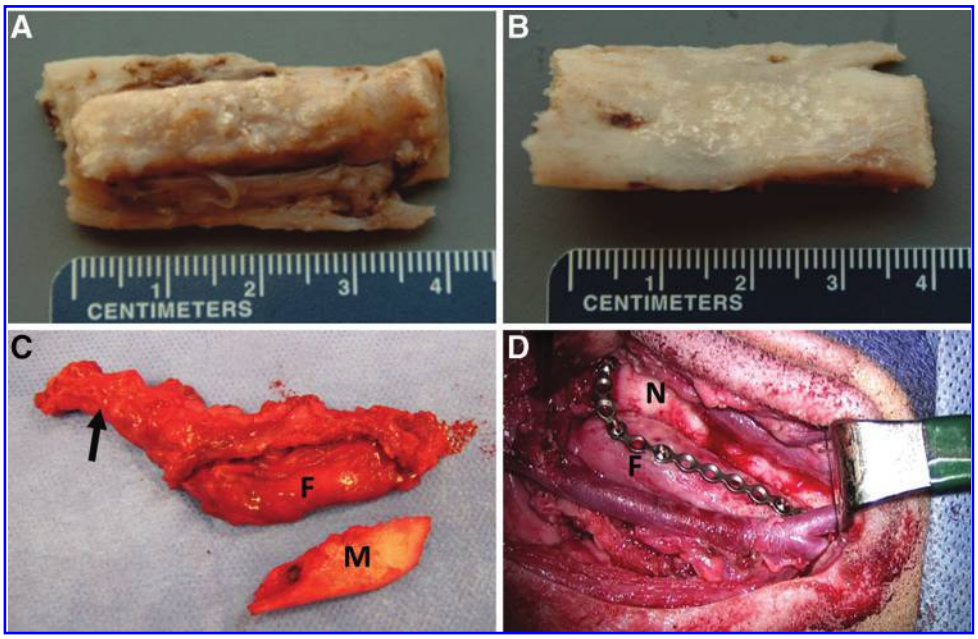

FIG. 3. Representative gross specimens after 9 weeks of implantation. **(A)** Top view of a 100% synthetic graft (SG) specimen **(B)** Bottom view of a 100% SG specimen. Notice the SG particles remaining on the underside of the specimen. **(C)** A flap and its subsequent transfer. F, flap; M, mandibular bone removed from defect creation, *Arrow*, vascular pedicle. **(D)** Transferred and plated flap. F, flap, N, native bone.

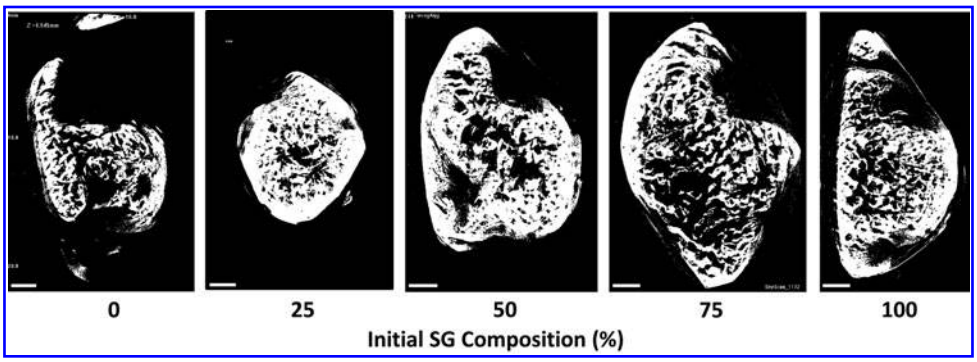

FIG. 4. Representative scans of tissue chamber specimens after 9 weeks of implantation (scale bar = 2000 μm).

of 10 μm. To examine the quality of bone, a region of interest was chosen within the specimen containing no overlap with areas outside of the chamber. The percentage of bone volume to total volume (BV/TV), trabecular number (Tb.N.), trabecular spacing (Tb.Sp.), and trabecular thickness (Tb.Th.) was calculated with CTAn software.

Histology

After scans, all samples were dehydrated in 70% ethanol. The tissue chamber specimens were embedded in methylmethacrylate, sliced in 10 μm sections along the Y-axis of the tissue chamber (Fig. 1A) using a microtome with a diamond blade (Leica Microsystems SP 1600, Nussloch, Germany), and subsequently stained with methylene blue/basic fuchsin. The mandibular specimens were embedded in methylmethacrylate, sliced in the coronal plane in 10 μm thick sections, and also stained with methylene blue/basic fuchsin. The sections were analyzed using light microscopy (Zeiss Axio Imager Z1 and AxioCam MRc 5; Carl Zeiss AG, Oberkochen, Germany). Fractional depth measurements were computed as described previously.[15] Briefly, the periosteum (or tissue at the open face of the chamber) was oriented as the X-axis. Perpendicular lines at 1/3, 1/2, and 2/3 the length of this line were drawn and the distance from the X-axis to the furthest living bone, as defined by viable osteocytes in lacunae, was measured at each point. These values were averaged and taken across three sections of each sample. The total average was taken per specimen and normalized by the height of the chamber (1 cm), resulting in the fractional depth measurement for that specimen. In addition, histomorphometry was performed to measure the percent surface area of remaining SG and newly formed bone. Briefly, the surface area of remaining SG and newly formed bone was traced and measured with ImageJ (National Institutes of Health, Washington, DC) and divided by

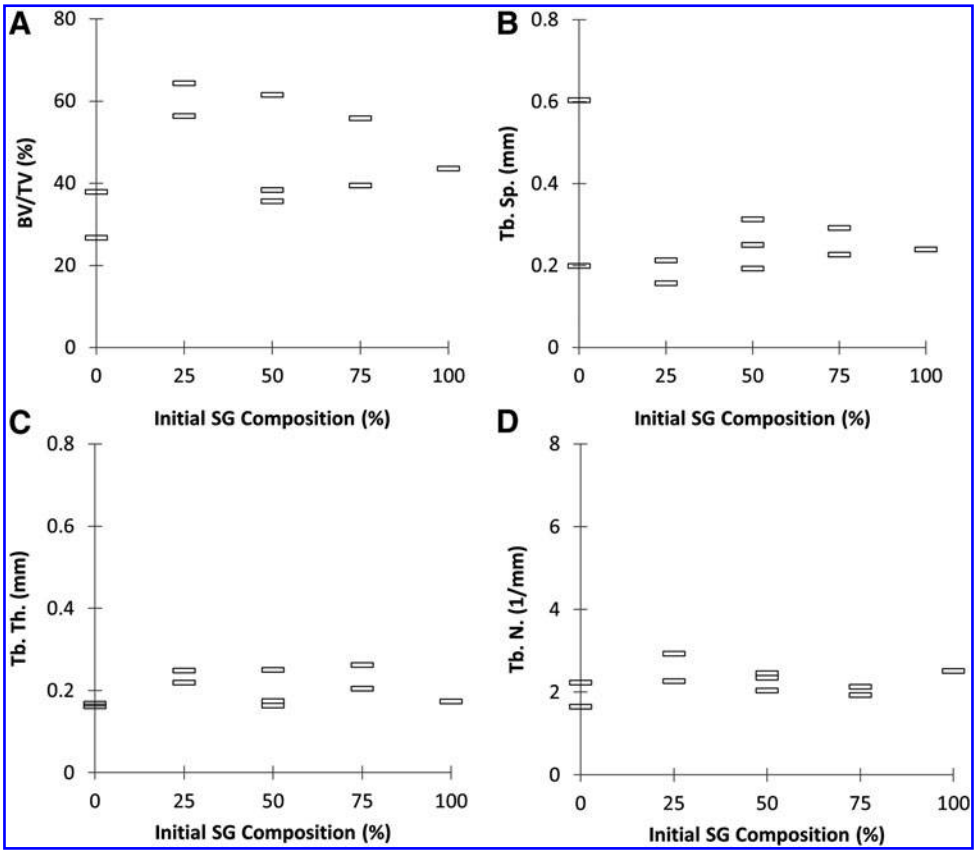

FIG. 5. Microcomputed tomography data as a function of initial SG composition ($n = 2, 2, 3, 2$, and 1 for groups with initial SG composition 0%, 25%, 50%, 75%, and 100%, respectively). **(A)** Percent bone volume/total volume (BV/TV). **(B)** Trabecular spacing (Tb.Sp.). **(C)** Trabecular thickness (Tb.Th.). **(D)** Trabecular number (Tb.N.).

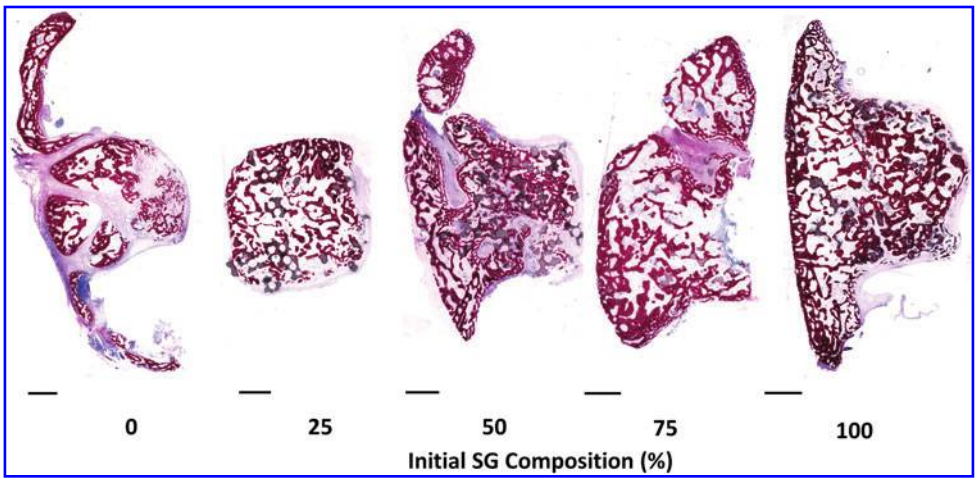

FIG. 6. Representative histologic images. These tissue chamber specimens have been implanted against rib periosteum for 9 weeks. The sections are oriented so that the left hand side of each specimen was the side adjacent to the periosteum and the right hand side was most distal to the periosteum upon implantation (scale bar = 2000 μm).

the total surface area of the tissue specimen grown within the implanted chamber. These measurements were performed on three sections per specimen and averaged to calculate the reported values of surface area of remaining SG and surface area of newly formed bone.

Results

Surgical recovery

All sheep recovered from the first surgery without complications. After the second surgery, one of the three sheep (100% AG flap) showed some facial edema, which resolved in ~1 week with no further intervention. All animals were able to ambulate and consume solid food the day following surgery.

Gross specimens

Two of the 16 rib chambers (chamber 1 in sheep 2 and chamber 3 in sheep 4) contained serous fluid upon harvest with no tissue ingrowth. Tissue filled the remaining chambers, roughly conforming to the dimensions of the chamber (Fig. 3A). Robust tissue growth occurred underneath the chambers and followed the contour of the chamber flap (Fig. 3B). The ossified tissue of chamber 4 in sheep 3 was accidently broken into two pieces upon chamber harvest. The larger piece was scanned by μCT, but this specimen was not used for fractional depth calculations. The intercostal artery and vein were able to be isolated and harvested as the flap pedicle (Fig. 3C). In all but one of the chambers with tissue, specimens had bone-like quality upon handling and were capable of supporting screws for plating (Fig. 3D). The contents of chamber 4 in sheep 4 were of fibrous consistency, which was later corroborated by μCT and histologic results (data not shown).

Microcomputed tomography

Specimens were scanned by μCT and analyzed to calculate BV/TV, Tb.N., Tb.Sp., and Tb.Th. (Figs. 4 and 5). Representative scans of specimens from each group of SG/AG ratio are presented in Figure 4. Significant differences between groups cannot be determined as the sample size of this pilot study is insufficient to perform statistical analysis.

Histology

Histological examination of the specimens from the tissue chambers revealed that ossified tissue generation occurred in all groups (Fig. 6). In specimens containing synthetic graft, there were gray regions within the tissue (Fig. 7) that resemble the histologic staining of beta-tricalcium phosphate-based materials seen in the literature.[25] These gray particles were absent in 100% AG-containing specimens (Fig. 8). In some regions, there appeared to be little new bone growth. For example, as seen in Figure 8A, sections of fragmented bone with no viable osteocytes surrounded by soft tissue could be seen in the apical region of the specimen, along with fibrous bands. In the same specimen, more robust bone

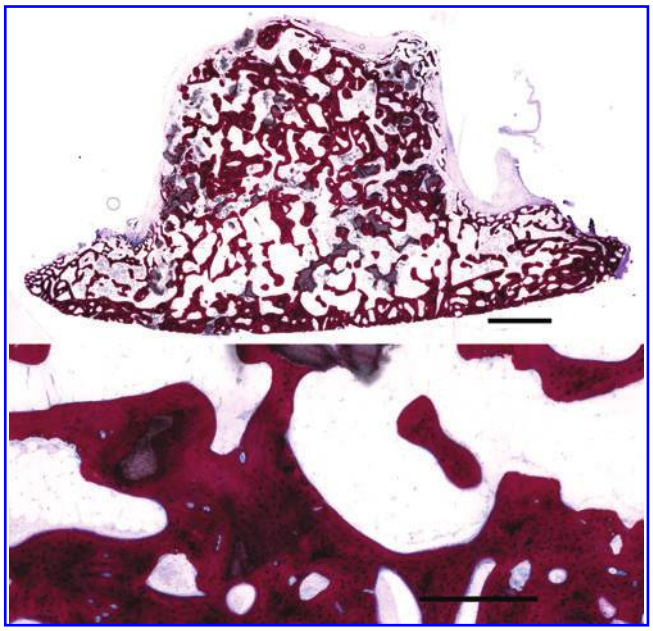

FIG. 7. Tissue chamber specimen with initial SG composition of 100%. Top: Low magnification view. For orientation, the bottom side was adjacent to the periosteum and the top side was most distal to the periosteum upon implantation (scale bar = 2000 μm). Bottom: High magnification section to demonstrate the osteointegration of SG particles with newly formed bone (scale bar = 500 μm).

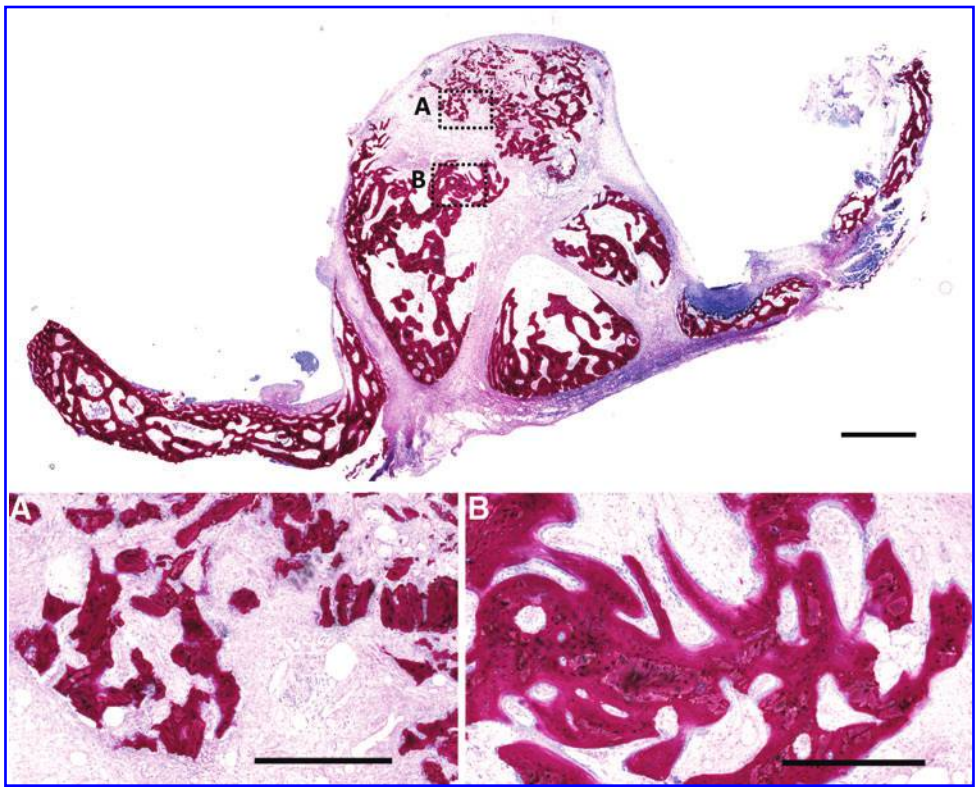

FIG. 8. Tissue chamber specimen with initial SG composition of 0%. Top: Low magnification view. For orientation, the bottom side was adjacent to the periosteum and the top side was most distal to the periosteum upon implantation (scale bar = 2000 μm). **(A)** Example of fragmented area with no live bone (scale bar = 500 μm). **(B)** Example of area with new bone growth as demonstrated by viable osteocytes and osteoblasts (scale bar = 500 μm).

growth can be seen in other regions (Fig. 8B). In many of the specimens, there was healthy growth of bone throughout the sample (Fig. 6). The synthetic graft particles appear to have become osteointegrated with the newly formed bone (Fig. 7). There does not appear to be a large effect of initial SG composition on the fractional depth, or height of viable bone grown within the chamber (Fig. 9), although this cannot be statistically calculated from the pilot study. Likewise, the percent surface areas of newly formed bone and remaining SG are reported in Figure 10.

Coronal sections of the mandibular flap reveal successful incorporation into the native bone (Fig. 11). In fact, it is difficult to distinguish native bone from the implanted flap at the defect borders. Compared to the contralateral control (left mandibular angle), the flap is much wider. This conforms to the initial geometries—the width of the tissue chamber is 1 cm, whereas the thickness of the sheep mandibular angle is ~0.5 cm. Grossly, there do not appear to be differences between the two 100% AG flaps and the one 100% SG flap in terms of integration. Both types of flaps exhibit small void spaces. SG particles can be seen remaining in the 100% SG flap (Fig. 11A). The SG appears to be osteointegrated with the newly formed bone, as demonstrated by bone growth around SG particles and within SG pores (Fig. 12).

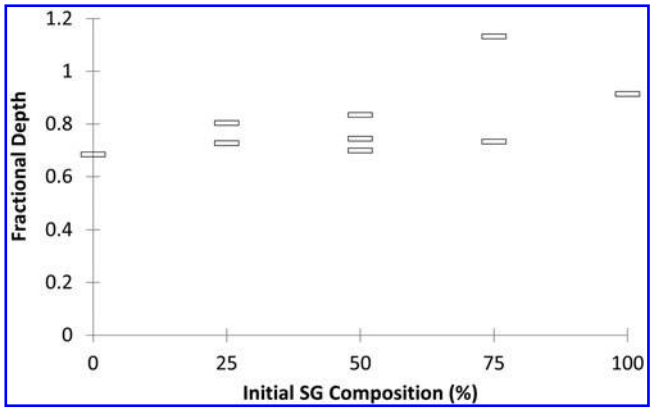

FIG. 9. Fractional depth as a function of initial synthetic bone graft composition ($n = 1, 2, 3, 2$, and 1 for groups with initial SG composition 0%, 25%, 50%, 75%, and 100%, respectively). The specimen scoring higher than 1 had such robust growth that new tissue displaced the chamber forward.

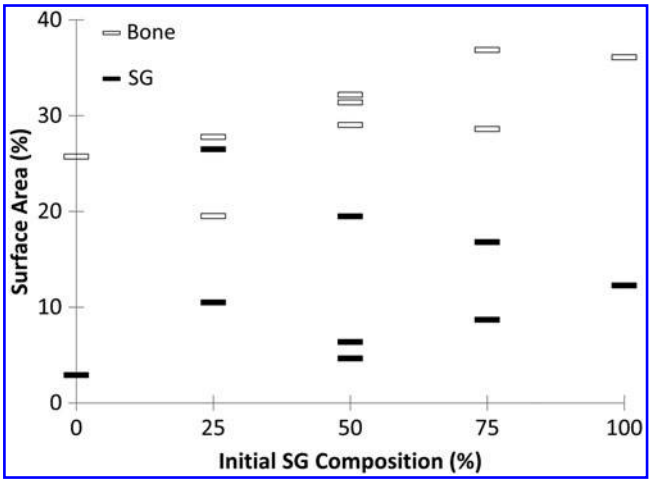

FIG. 10. Percent surface area of bone within the chambers (*white* markers) and remaining SG (*black* markers).

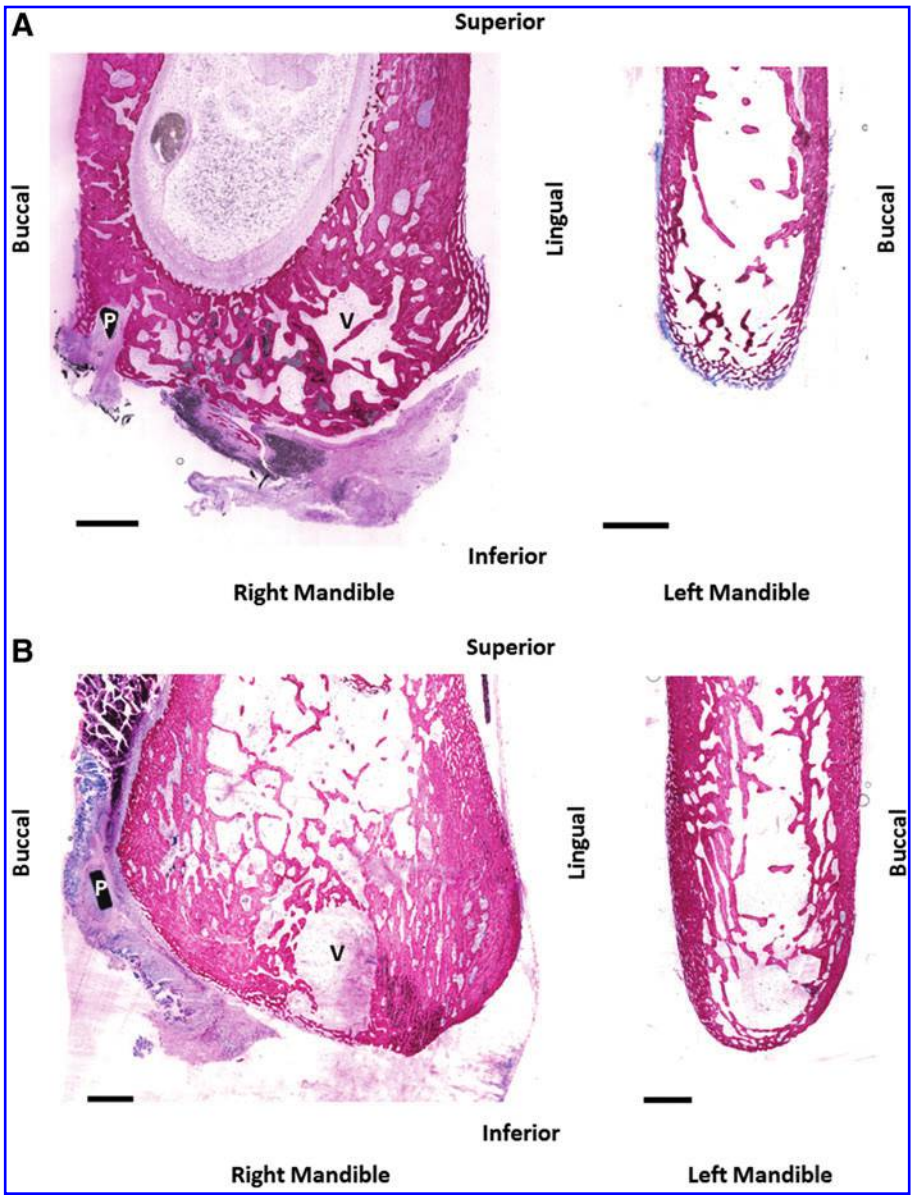

FIG. 11. Mandibular angles 12 weeks after free flap transfer. **(A)** 100% SG flap. P, plate; V, void space. The left mandible is a contralateral control (scale bars = 2000 μm). **(B)** 0% SG flap. P, plate; V, void space. The left mandible is a contralateral control (scale bars = 2000 μm).

Discussion

The ability to autologously generate a tissue-engineered bone flap of customizable dimensions for transfer into craniofacial defects, without the aid of exogenous growth factors, would represent a major advancement in the field. While the feasibility of generating these flaps orthotopically has previously been described and optimized in this sheep model,[15–19] transfer into a mandibular defect had not been demonstrated in the literature. In addition, the use of synthetic bone graft as a scaffold in place of autograft could result in the mitigation of donor site morbidity for the clinical translation of this approach. In this study, tissue chambers with different ratios of autograft and synthetic bone graft were

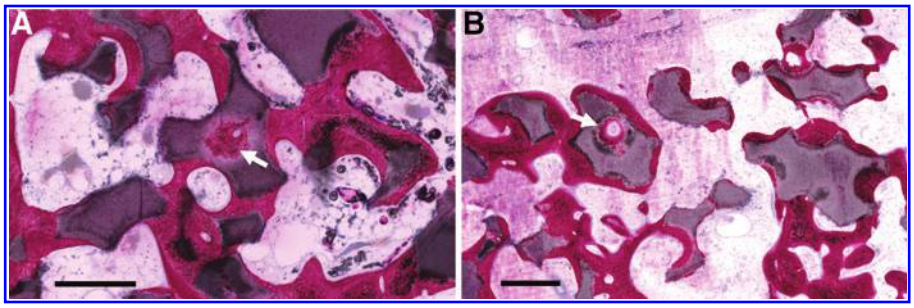

FIG. 12. Examples of bone growth within SG pores (scale bars = 500 μm). *Arrow*, pore. **(A)** SG within a transferred mandibular flap. **(B)** SG within a tissue chamber specimen.

prepared and implanted on the periosteum of sheep rib for 9 weeks. While this pilot study did not have a sufficiently high sample size to perform statistical comparisons, the use of synthetic bone graft did not appear to diminish the quantity or quality of bone generated as assessed by μCT parameters and histological measurements (Figs. 5, 9, and 10).

When analyzing the μCT data (Fig. 5), it is important to note that the trabecular indices (Tb.Sp., Tb.Th., and Tb.N.) are intended for trabeculae and not necessarily the ossified tissue-engineered construct that is grown within these implanted chambers. In another ovine study, trabecular bone samples were obtained from sheep femoral condyles and grouped by mechanical strength. It was found that greater trabecular bone strength is positively correlated with BV/TV, Tb.N., Tb.Th., and negatively correlated with Tb.Sp.[26] Similar relationships have been reported in human bone studies.[27] The mean values of the ovine measurements, pooling all groups together ($n=45$), were reported as $28\% \pm 7\%$, $1.70 \pm 0.13\,mm^{-1}$, 0.53 ± 0.05 mm, and 0.19 ± 0.05 mm for BV/TV, Tb.N., Tb.Sp., and Tb.Th., respectively.[26] When pooling together specimens from all groups in this pilot study ($n=10$), the mean values were $46\% \pm 13\%$, $2.25 \pm 0.35\,mm^{-1}$, 0.27 ± 0.13 mm, and 0.20 ± 0.04 mm for BV/TV, Tb.N., Tb.Sp., and Tb.Th., respectively. Comparing these results, the tissue grown in the chamber had greater BV/TV and Tb.N., similar Tb.Th., and smaller Tb.Sp. than the average values of tissue from sheep femoral condyles. Based on the correlation of bone strength with these μCT parameters, it is possible that the tissue generated in the implanted chambers has greater mechanical strength than pure trabecular bone and may be more similar to corticocancellous bone. In future studies, mechanical testing will be performed on specimens to further explore the nature of the generated tissue.

The fractional depth measurements reported in this study (Fig. 9) are within the values previously reported for morcellized autologous bone and exceed the values reported for empty chambers and devitalized bone.[16] The SG particles appear to partially degrade over time, as illustrated by the minimization of SG and appearance of new bone in tissue chambers that were initially filled completely with SG particles (Fig. 7). While statistics cannot be performed due to the small sample size, the inclusion of SG does not appear to diminish the percent surface area of bone formed within the chambers (Fig. 10).

In our study, regions of SG remain in tissue chambers at 9 weeks and in a flap transferred to the mandible after a total of 21 weeks ($\sim$5 months) *in vivo*. These regions demonstrate osteointegration of the SG by newly grown bone and appear to incorporate well into the native bone architecture (Figs. 11 and 12). This corroborates with other *in vivo* studies, which have noted the continued presence of this SG with some degradation over a similar time scale.[23,28] As these particular SG particles are composed of 85% beta-tricalcium phosphate and 15% hydroxyapatite, it is possible there was some early resorption as this biphasic material is more readily degradable than pure hydroxyapatite graft.[21] The release of calcium and phosphates from this degradation may aid osteoconduction and osteoinduction,[24] resulting in the bone formation seen in these results. In the two chambers with serous fluid and limited tissue ingrowth, it is possible that the fragile cambium layer of the periosteum, where the majority of mesenchymal stem cells reside,[29] was damaged during insertion of the tissue chamber. Experience with this procedure may reduce this negative outcome (seen in 2/16 chambers).

In this study, flap transfer from these tissue chambers was successful in all animals (3/3), regardless of initial scaffold composition within the chambers. Flap integration with native bone after insertion into a mandibular angle defect was observed by histology. While central necrosis is often seen in large bone grafts due to lack of nutrient and oxygen diffusion, the anastomosis of the flap with local vasculature allowed for viable tissue almost completely throughout the region, with only a small void space (Fig. 11). In this study, all sheep tolerated both stages of the procedure well. The flap transferred with SG showed healthy integration, with bone encapsulating particles and growing within particle pores (Figs. 11 and 12). As demonstrated by the width of the right mandible compared with the contralateral control side, the transferred tissue retained some of its initial geometry. However, when grossly comparing the contents of the tissue chambers at 9 weeks to the mandibular flaps 12 weeks later, it is clear that significant remodeling had taken place within the flap. To minimize potential tissue disturbance, the surgical plate was kept in place for histology and therefore μCT was not successfully performed due to scanning artifacts from the plate. However, in future studies, the plate will be removed after harvest and the mandibles will be subjected to μCT, allowing for more quantitative data on flap remodeling by measurements such as BV/TV and mandibular ridge width compared to the contralateral control.

Conclusion

This study demonstrates the feasibility of transferring a tissue-engineered vascularized bone flap grown in an autologous *in vivo* bioreactor to a defect site. Flap generation was possible using either autologous bone, synthetic bone graft, or a combination of the two. After transferring flaps that were originally either 100% autologous bone or 100% synthetic bone graft into a mandibular angle defect, it was seen that both types of flaps remained viable after 12 weeks in 3/3 animals. This growth factor free strategy is an appealing approach to the complex problem of large craniofacial defect reconstruction.

Acknowledgments

We would like to acknowledge support from the Louis Calder Professorship of Rice University (A.G.M.) for this study, as well as from the National Institutes of Health (R01 AR048756 and R01 AR057083) and the Armed Forces Institute of Regenerative Medicine (W81XWH-14-2-0004) for research in the area of bone tissue engineering. We would also like to acknowledge KLS Martin for the use of a bone mill and Leica Microsystems for use of a surgical microscope. We would also like to thank Ms. Natasja van Dijk for her assistance with histological sectioning and staining and Mr. Adam Wilson for his assistance in animal care. A.M.T. would like to thank the Baylor College of Medicine Medical Scientist Training Program (NIH T32 GM007330) and the Barrow Scholars Program.

Disclosure Statement

No competing financial interests exist.

References

1. Bak, M., Jacobson, A.S., Buchbinder, D., and Urken, M.L. Contemporary reconstruction of the mandible. Oral Oncol **46,** 71, 2010.
2. Hayden, R.E., Mullin, D.P., and Patel, A.K. Reconstruction of the segmental mandibular defect: current state of the art. Curr Opin Otolaryngol Head Neck Surg **20,** 231, 2012.
3. Klotch, D.W., Gump, J., and Kuhn, L. Reconstruction of mandibular defects in irradiated patients. Am J Surg **160,** 396, 1990.
4. Petersen, K., Hayes, D.K., Blice, J.P., and Hale, R.G. Prevention and management of infections associated with combat-related head and neck injuries. J Trauma **64,** S265, 2008.
5. Foster, R.D., Anthony, J.P., Sharma, A., and Pogrel, M.A. Vascularized bone flaps versus nonvascularized bone grafts for mandibular reconstruction: an outcome analysis of primary bony union and endosseous implant success. Head Neck **21,** 66, 1999.
6. Cordeiro, P.G., Disa, J.J., Hidalgo, D.A., and Hu, Q.Y. Reconstruction of the mandible with osseous free flaps: a 10-year experience with 150 consecutive patients. Plast Reconstr Surg **104,** 1314, 1999.
7. Kroll, S.S., Schusterman, M.A., Reece, G.P., Miller, M.J., Evans, G.R., Robb, G.L., *et al.* Choice of flap and incidence of free flap success. Plast Reconstr Surg **98,** 459, 1996.
8. Tatara, A.M., Wong, M.E., and Mikos, A.G. *In vivo* bioreactors for mandibular reconstruction. J Dent Res **93,** 1196, 2014.
9. McCullen, S.D., Chow, A.G., and Stevens, M.M. *In vivo* tissue engineering of musculoskeletal tissues. Curr Opin Biotechnol **22,** 715, 2011.
10. Henslee, A.M., Spicer, P.S., Shah, S.R., Tatara, A.M., Kasper, F.K., Mikos, A.G., *et al.* Use of porous space maintainers in staged mandibular reconstruction. oral and maxillofacial surgery clinics of North America **26,** 143, 2014.
11. Heliotis, M., Lavery, K.M., Ripamonti, U., Tsiridis, E., and di Silvio, L. Transformation of a prefabricated hydroxyapatite/osteogenic protein-1 implant into a vascularised pedicled bone flap in the human chest. Int J Oral Maxillofac Surg **35,** 265, 2006.
12. Warnke, P.H., Springer, I.N., Wiltfang, J., Acil, Y., Eufinger, H., Wehmoller, M., *et al.* Growth and transplantation of a custom vascularised bone graft in a man. Lancet **364,** 766, 2004.
13. Orringer, J.S., Shaw, W.W., Borud, L.J., Freymiller, E.G., Wang, S.A., and Markowitz, B.L. Total mandibular and lower lip reconstruction with a prefabricated osteocutaneous free flap. Plast Reconstr Surg **104,** 793, 1999.
14. Boraiah, S., Paul, O., Hawkes, D., Wickham, M., and Lorich, D.G. Complications of recombinant human BMP-2 for treating complex tibial plateau fractures: a preliminary report. Clin Orthop Relat Res **467,** 3257, 2009.
15. Miller, M.J., Goldberg, D.P., Yasko, A.W., Lemon, J.C., Satterfield, W.C., Wake, M.C., *et al.* Guided bone growth in sheep: a model for tissue-engineered bone flaps. Tissue Eng **2,** 51, 1996.
16. Cheng, M.H., Brey, E.M., Allori, A., Satterfield, W.C., Chang, D.W., Patrick, C.W., Jr., *et al.* Ovine model for engineering bone segments. Tissue Eng **11,** 214, 2005.
17. Brey, E.M., Cheng, M.H., Allori, A., Satterfield, W., Chang, D.W., Patrick, C.W., Jr., *et al.* Comparison of guided bone formation from periosteum and muscle fascia. Plast Reconstr Surg **119,** 1216, 2007.
18. Thomson, R.C., Mikos, A.G., Beahm, E., Lemon, J.C., Satterfield, W.C., Aufdemorte, T.B., *et al.* Guided tissue fabrication from periosteum using preformed biodegradable polymer scaffolds. Biomaterials **20,** 2007, 1999.
19. Cheng, M.H., Brey, E.M., Allori, A.C., Gassman, A., Chang, D.W., Patrick, C.W., Jr., *et al.* Periosteum-guided prefabrication of vascularized bone of clinical shape and volume. Plast Reconstr Surg **124,** 787, 2009.
20. Cheng, M.H., Brey, E.M., Ulusal, B.G., and Wei, F.C. Mandible augmentation for osseointegrated implants using tissue engineering strategies. Plast Reconstr Surg **118,** 1e, 2006.
21. Moore, W.R., Graves, S.E., and Bain, G.I. Synthetic bone graft substitutes. ANZ J Surg **71,** 354, 2001.
22. Kagami, H., Agata, H., Inoue, M., Asahina, I., Tojo, A., Yamashita, N., *et al.* The use of bone marrow stromal cells (bone marrow-derived multipotent mesenchymal stromal cells) for alveolar bone tissue engineering: basic science to clinical translation. Tissue Eng Part B Rev **20,** 229, 2014.
23. Wakimoto, M., Ueno, T., Hirata, A., Iida, S., Aghaloo, T., and Moy, P.K. Histologic evaluation of human alveolar sockets treated with an artificial bone substitute material. J Craniofac Surg **22,** 490, 2011.
24. LeGeros, R.Z., Lin, S., Rohanizadeh, R., Mijares, D., and LeGeros, J.P. Biphasic calcium phosphate bioceramics: preparation, properties and applications. J Mater Sci Mater Med **14,** 201, 2003.
25. Yuan, H., Fernandes, H., Habibovic, P., de Boer, J., Barradas, A.M., de Ruiter, A., *et al.* Osteoinductive ceramics as a synthetic alternative to autologous bone grafting. Proc Natl Acad Sci U S A **107,** 13614, 2010.
26. Mittra, E., Rubin, C., and Qin, Y.X. Interrelationship of trabecular mechanical and microstructural properties in sheep trabecular bone. J Biomech **38,** 1229, 2005.
27. Goulet, R.W., Goldstein, S.A., Ciarelli, M.J., Kuhn, J.L., Brown, M.B., and Feldkamp, L.A. The relationship between the structural and orthogonal compressive properties of trabecular bone. J Biomech **27,** 375, 1994.
28. Herford, A.S., Lu, M., Buxton, A.N., Kim, J., Henkin, J., Boyne, P.J., *et al.* Recombinant human bone morphogenetic protein 2 combined with an osteoconductive bulking agent for mandibular continuity defects in nonhuman primates. J Oral Maxillofac Surg **70,** 703, 2012.
29. Chang, H., Knothe and Tate, M.L. Concise review: the periosteum: tapping into a reservoir of clinically useful progenitor cells. Stem Cells Transl Med **1,** 480, 2012.

Address correspondence to:
Antonios G. Mikos, PhD
Department of Bioengineering
Rice University
MS142
BioScience Research Collaborative
6500 Main Street
Houston, TX 77030

E-mail: mikos@rice.edu

Received: July 16, 2014
Accepted: January 7, 2015
Online Publication Date: February 27, 2015